






Manipulating the radial components of LG pump beam for ultrahigh-dimensional maximally entangled orbital angular momentum states

CHUAN XU,¹ LINTAO XIAO,¹ JIANLANG HE,¹ HAN ZHANG,^{1,4}
DUNZHAO WEI,² XIAOPENG HU,¹  MIN XIAO,^{1,3}  AND YONG
ZHANG^{1,5} 

¹National Laboratory of Solid State Microstructures, College of Engineering and Applied Sciences, School of Physics, and Collaborative Innovation Center of Advanced Microstructures, Nanjing University, Nanjing 210093, China

²School of Physics, Sun Yat-sen University, Guangzhou 510275, China

³Department of Physics, University of Arkansas, Fayetteville, Arkansas 72701, USA

⁴zhanghan@nju.edu.cn

⁵zhangyong@nju.edu.cn

Abstract: High-dimensional maximally entangled orbital angular momentum (OAM) states are a promising resource for enhancing information capacity and robustness in quantum communication. However, it still lacks an effective method to increase the state dimensionality. Here, we theoretically propose an efficient scheme to generate maximally entangled OAM states of ultrahigh dimensionality by manipulating the radial components of a Laguerre-Gaussian (LG) pump beam. By optimizing the complex amplitudes of multiple radial modes of the LG pump light, one can feasibly achieve 101-dimensional OAM-based maximally entangled states. Our scheme has potential applications in high capacity quantum communication networks.

© 2022 Optica Publishing Group under the terms of the [Optica Open Access Publishing Agreement](#)

1. Introduction

High-dimensional maximally entangled states (MESs) of two photons have raised widespread interests because of their promising applications, such as closing the detection loophole in Bell test experiments, enhancing information capacity, and raising the resistance to noise in quantum communication [1–3]. In generating MESs, various degrees of freedom such as which-way paths, discretized time and frequency modes, and transverse-spatial modes can be used [4–9].

The entanglement of Laguerre-Gaussian (LG) modes has been extensively studied because these modes carry OAM quanta [10]. The discrete nature of OAM in infinite-dimensional Hilbert space is quite suitable for high-dimensional quantum information. To date, the OAM of light has become a workhorse for high-dimensional spatial-mode-based MESs, which can be generated and manipulated conveniently in nonlinear optical processes [7,11–15]. In a nonlinear crystal, an intense pump light produces two entangled photons (referred to as signal and idler) through a spontaneous parametric down-conversion (SPDC) process, which obeys the conservation laws of energy, momentum, and OAM [16]. The main methods to generate high-dimensional OAM-based MESs are entanglement concentration (i.e., Procrustean filtering) [7,17] and pump light shaping (which manipulates the spatial modes of the pump light) [18–20]. The entanglement concentration method requires a broad spiral bandwidth to realize high-dimensional entanglement, which is difficult to be satisfied by using a traditional Gaussian pump beam. By shaping the LG pump light, several groups have successfully broadened the spiral bandwidth and efficiently produced arbitrary three-dimensional OAM-based MESs. These works mainly manipulate the azimuthal components (i.e., OAM quantum number l) of the pump light. However, such pump light carrying multiple OAM components usually produce unwanted photon modes during

SPDC, which requires extra diagonalization of the OAM detection bases [19,20]. The higher the dimensionality of the state is, the more cumbersome the manipulation is.

In this paper, we theoretically propose a scheme to generate executable ultrahigh-dimensional OAM-based MESs efficiently by manipulating the radial components p of LG pump light. The OAM spectrum of two-photon states is dependent on the spatial shape of the pump light [18–22]. In our scheme, the azimuthal component of the pump light is fixed to be $l = 0$, which well avoids the requirement of detection base diagonalization in previous works. Using gradient descent and simulated annealing algorithms [23], we numerically simulate the optimal complex amplitudes of the p components of LG pump light to produce high-dimensional OAM-based MESs. By constructing proper LG pump light with six p components [24], we obtain OAM-based MESs from three dimensions to twenty dimensions with high accuracies. Furthermore, with an LG pump light consisting of seventeen p modes, 101-dimensional OAM-based MESs can be achieved, which has potential applications in high-capacity robust quantum networks. Our scheme can also be applied in quantum state engineering such as the generation of two-photon states with symmetric OAM spectra.

2. Principle

In a SPDC, signal and idler photons are strongly OAM-correlated through the conservation law of OAM [16]. Moreover, the OAM coincidence probability of the entangled two-photon state, i.e., the spiral spectrum [25], is not uniform because the coincidence probability depends on the overlap between the spatial modes of the entangled photons and the pump light. Here, we consider an ideally-phase-matched collinear SPDC process. For completeness of the LG base, the entangled two-photon state of the spatial modes in a thin crystal is [26]

$$|\psi\rangle = \sum_{l_s, p_s} \sum_{l_i, p_i} C_{p_s, p_i}^{l_s, l_i} |l_s, p_s; l_i, p_i\rangle, \quad (1)$$

with the coincidence probability amplitude $C_{p_s, p_i}^{l_s, l_i}$ being

$$\begin{aligned} C_{p_s, p_i}^{l_s, l_i} &= \frac{\sqrt{2p_p! p_s! p_i! (|l_p| + p_p)! (|l_s| + p_s)! (|l_i| + p_i)!}}{\sqrt{\pi} w_p} \\ &\times \left(\frac{2}{1 + \gamma_s^2 + \gamma_i^2} \right)^{\frac{|l_p| + |l_s| + |l_i|}{2} + 1} \gamma_s^{|l_s| + 1} \gamma_i^{|l_i| + 1} \delta_{l_p, l_s + l_i} \\ &\times \sum_{j_p=0}^{p_p} \sum_{j_s=0}^{p_s} \sum_{j_i=0}^{p_i} \frac{\left(-\frac{2}{1 + \gamma_s^2 + \gamma_i^2} \right)^{j_p + j_s + j_i} \gamma_s^{2j_s} \gamma_i^{2j_i} \left[\frac{|l_p| + |l_s| + |l_i|}{2} + j_p + j_s + j_i \right]!}{(|l_s| + j_s)! j_s! (p_s - j_s)! (|l_i| + j_i)! j_i! (p_i - j_i)! (|l_p| + j_p)! j_p! (p_p - j_p)!}, \end{aligned} \quad (2)$$

where γ denotes the width ratio of the pump (w_p) to the entangled photon, and the subscript s (i) signifies the detected signal (idler) photon. The Kronecker delta function $\delta_{l_p, l_s + l_i}$ ensures the OAM conservation law. The labels l and p denote the OAM (azimuthal) and radial node numbers of the LG mode, respectively. For simplicity, we assume that the OAM number of the LG pump light is zero, i.e., $l_p = 0$, and the spatial modes of the coincidence detection base maintain $p_s = p_i = 0$, $\gamma_s = \gamma_i = \gamma = 1$ and $l_s, l_i = -50, -49, \dots, 50$. This setting is valid unless otherwise noted.

To produce high-dimensional OAM-based MESs, the spatial mode of the pump light is a coherent superposition state $|\psi\rangle_p$ consisting of LG modes with the same l_p but different p_p . $|\psi\rangle_p$

is given as

$$|\psi\rangle_p = \sum_{p_p} C_{p_p} |l_p = 0, p_p\rangle, \quad (3)$$

where C_{p_p} denotes the complex amplitude. We calculate the distribution of the coincidence probability amplitude $C_{p_s, l_i}^{l_s, l_i}$ when the pump light is a single LG mode within $p_p = 0, 1, \dots, 5$ [Fig. 1(a)]. All the spectra of the coincidence probability amplitudes are symmetric and centered at $l_s = 0$. When $p_p \neq 0$, negative values of $C_{p_s, l_i}^{l_s, l_i}$ arise from the non-uniform phase of the pump light.

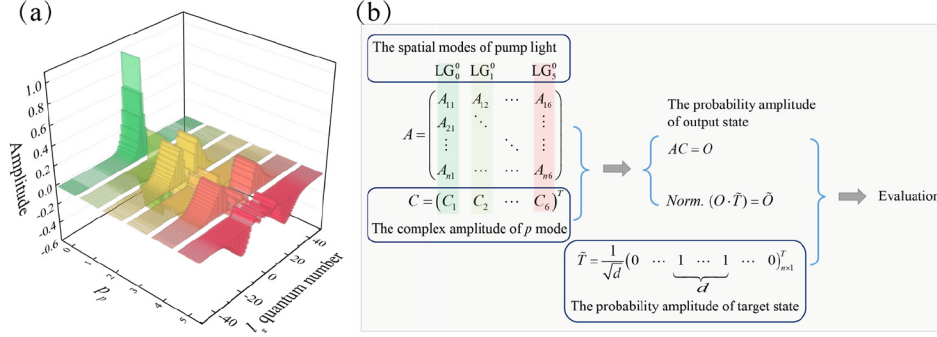


Fig. 1. (a) Normalized spectra of the coincidence probability amplitudes with $l_p = 0$ and $p_p = 0, 1, \dots, 5$. (b) Outline of the generation scheme for d -dimensional OAM-based MES. \tilde{T} denotes the amplitude of target state $|\psi\rangle_T$. The superscript and subscript appended to LG denote quantum numbers l_p and p_p , respectively. *Norm.* is the normalization function. O and \tilde{O} denote the coincidence probability amplitudes of output and desired states, respectively.

From the data in Fig. 1(a), we construct the matrix A consisting of six spectra of the coincidence probability amplitudes [Fig. 1(b)], in which the columns and rows refer to the LG components of the pump light ($p_p = 0, 1, \dots, 5$) and the OAM numbers of the detected photon pairs ($l_s, l_i = -50, -49, \dots, 50$), respectively. The complex amplitude vector of the LG pump light is defined as $C = (C_1, C_2, \dots, C_6)^T$, and the target state of the d -dimensional OAM MES is given as $|\psi\rangle_T = \frac{1}{\sqrt{d}} \sum_l |l, -l\rangle$. In Fig. 1(b), the amplitude of the target state is set as the vector \tilde{T} . For odd d , the spatial modes of the d -dimensional target state $|\psi\rangle_T$ are $l = -(d-1)/2, -(d-1)/2+1, \dots, (d-1)/2$. For even d , the spatial modes of the target state $|\psi\rangle_T$ are $l = -d/2, \dots, -1, 1, \dots, d/2$. From the product of A and C , we obtain the vector O which denotes the coincidence probability amplitude of the two-photon output state $|\psi\rangle_O$. By post-selecting the modes of $|\psi\rangle_T$ from $|\psi\rangle_O$, we obtain the desired state $|\tilde{\psi}\rangle_O$. \tilde{O} denotes the amplitude of $|\tilde{\psi}\rangle_O$, which should be as close to \tilde{T} as possible.

With the gradient descent and simulated annealing algorithms, we find the optimal amplitude vector C to produce $|\tilde{\psi}\rangle_O$ efficiently and accurately. We first create the evaluation function E , i.e.,

$$E = E_1 + E_2, \quad (4)$$

with

$$E_1 = \sum_i (\tilde{O}_i - \tilde{T}_i)^2, \quad (5)$$

$$E_2 = \sum_i (O_i - \tilde{T}_i)^2. \quad (6)$$

Here, all \tilde{T}_i are positive (i.e., all \tilde{T}_i are in-phase). The function E_1 (E_2) is used to evaluate the similarity between \tilde{O} (O) and \tilde{T} . The smaller the value of the function E_1 (E_2), the more accurate (efficient) the desired state $|\tilde{\psi}\rangle_O$ is. Then, at each iteration, the amplitude vector changes by a small amount of

$$\Delta C_i = \frac{\eta \left[\sum_j (\tilde{T}_j - \tilde{O}_j) A_{ji} + T \sum_j (\tilde{T}_j - O_j) A_{ji} \right]}{1 + T}, \quad (7)$$

where η denotes the descending rate of the error and T the computational temperature. The cost function \bar{C} obeys $\bar{C} \propto \frac{E_1 + T E_2}{1 + T}$. For three-dimensional to twenty-dimensional entanglements, the initial and final temperatures and the descending rate of change in temperature are chosen as 10^{50} , 10^{-50} , and 0.997, respectively. The final temperature here is obtained from the loop termination condition. When the temperature T is high (or low), the direction of change in ΔC_i and the cost function are used to produce an efficient (or accurate) output. For an arbitrary initial amplitude vector, an optimal solution can be obtained.

3. Experimental scheme and simulation

We propose an experimental scheme for the generation of high-dimensional OAM-based MESs (Fig. 2). A phase-only spatial light modulator1 (SLM1) realizes a complex-field modulation of the pump light, which is then injected into a BBO crystal [24]. One can generate the complex field with high fidelity by use of phase-amplitude encoding [27–31]. In this nonlinear crystal, a 415-nm pump light produces two entangled photons with the same polarizations, corresponding to a type-I SPDC process. We use lenses and single-mode fibers (SMFs) to control γ_s and γ_i . Moreover, SLM 2 and SLM 3 are used to project the photons into the detection base and convert the specific spatial component of the photons into a Gaussian mode. To further improve the detection accuracy, one should consider the filtering effect from SMF and correct the holograms by a Gaussian mode function [32–35]. Then, SMFs collect the photons in Gaussian modes, avalanche photodiodes detect the delivered photons and a coincidence count takes place. For d -dimensional OAM-based MESs, where $d = 3, 4, \dots, 20$, we calculate the complex amplitudes of the six LG modes of the pump light (Table 1). The corresponding OAM-based MESs are given in Fig. 3(a) marked with red bars. In Table 1, negative signs indicate a π phase delay.

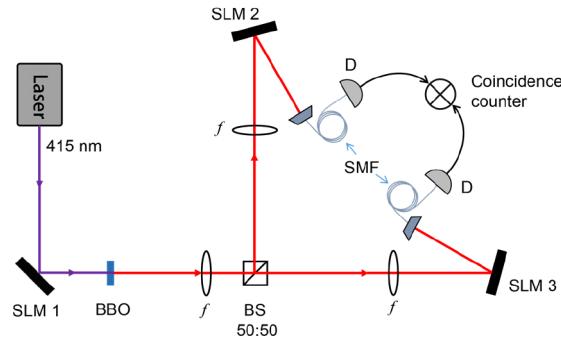


Fig. 2. Experimental scheme for the generation of high-dimensional OAM-based MESs. SLM, spatial light modulator; SMF, single-mode fiber; BS, beam splitter; D, detector with avalanche photodiodes.

For these OAM-based MESs, the mean square errors of the coincidence probability amplitudes between \tilde{O} and \tilde{T} , i.e., $\frac{E_i}{d}$ are less than 10^{-6} [Fig. 3(b)]. The curves of the mean square error and fidelity confirm the high accuracy between \tilde{O} and \tilde{T} . In the detection base, we calculate the angular Schmidt numbers of the output states $|\psi\rangle_O$ [Fig. 3(c)]. With the growing dimensionality

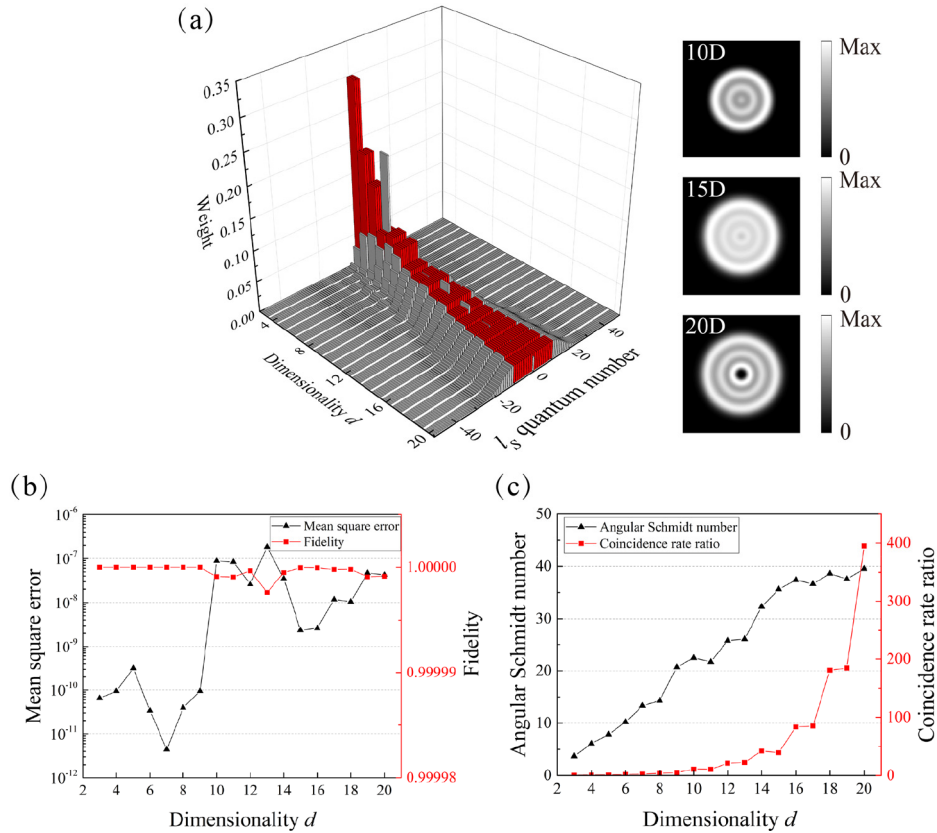


Fig. 3. (a) Normalized spiral spectra of the output states $|\psi\rangle_O$. The OAM-based MESs range from three-dimensional to twenty-dimensional spaces. Here, normalization is performed on each detection base. Red bars denote the desired modes. For even d , the spatial modes of the target state $|\psi\rangle_T$ do not contain the mode of $|0\rangle_s|0\rangle_i$, i.e., the mode of $|0\rangle_s|0\rangle_i$ is not optimized by the algorithm. So there exists a dip or a peak for the state of $|0\rangle_s|0\rangle_i$ in even dimension. The profiles of the optimal pump beam for 10D, 15D, 20D MESs are also presented. (b) The dependence of the mean square error and fidelity between \tilde{O} and \tilde{T} on the dimensionality d . (c) The dependence of the angular Schmidt number of $|\psi\rangle_O$ and the coincidence rate ratio on the dimensionality d in the detection base with $p_s = p_i = 0$. Here, the coincidence rate ratio is the coincidence rate of our method to that of entanglement concentration.

Table 1. The calculated complex amplitudes of the p components of pump light (with $l_p = 0$) for the generations of various high-dimensional OAM MESs.

Dimensionality	$p_p = 0$	$p_p = 1$	$p_p = 2$	$p_p = 3$	$p_p = 4$	$p_p = 5$
	Complex amplitude					
3D	0.4627	0.1064	-0.2389	-0.5198	-0.5871	-0.3203
4D	0.1035	-0.5353	-0.6991	-0.4237	0.0337	0.1826
5D	0.5351	-0.2185	-0.3522	0.0479	0.5554	0.4807
6D	0.6843	-0.2479	0.1048	0.5822	0.2271	-0.2624
7D	0.6061	-0.4897	0.0666	0.4109	-0.0683	-0.4636
8D	0.3063	-0.6373	-0.0034	0.0685	-0.4614	-0.5314
9D	0.5915	-0.5695	0.4458	-0.118	-0.2447	0.2307
10D	0.5779	-0.5776	0.4844	-0.2532	-0.0935	0.1578
11D	0.5749	-0.5598	0.4657	-0.1809	-0.2011	0.2572
12D	0.5776	-0.4972	0.533	-0.3108	0.1065	0.1647
13D	0.5551	-0.5488	0.505	-0.348	0.0718	0.0969
14D	0.5261	-0.4843	0.5082	-0.3979	0.2673	-0.0234
15D	0.4884	-0.4873	0.4776	-0.432	0.3075	-0.1214
16D	0.4661	-0.4841	0.4595	-0.4467	0.3294	-0.1713
17D	0.4795	-0.4788	0.4719	-0.4361	0.3275	-0.1441
18D	0.4473	-0.4855	0.4429	-0.458	0.3377	-0.2103
19D	0.4716	-0.4712	0.4661	-0.4381	0.3439	-0.1676
20D	0.4295	-0.4893	0.4263	-0.4683	0.3394	-0.2447

of MESs, the spiral bandwidth becomes broader, and the angular Schmidt numbers are always larger than the corresponding d . To compare our method with entanglement concentration, we plot the curve of the coincidence rate ratio of our method to that of entanglement concentration [Fig. 3(c)]. Here, the coincidence rate of entanglement concentration is calculated with pump light settings $l_p = p_p = 0$ and $\gamma = 1$. Note that the entanglement concentration method is efficient when $d < 6$. For higher dimensions, the high-order modes of the pump light having wide spiral bandwidths are fully utilized and the coincidence rate improvement in our method becomes notable. To further increase the coincidence rate and accuracy of the generated state, one can increase the p mode number of the LG pump light, optimize parameters γ_s and γ_i , or increase the iteration number of the algorithm.

It is known that the parameter γ should be set as large as possible to produce high-dimensional OAM-based MESs by entanglement concentration. However, $\gamma \gg 1$ cannot be achieved in an experiment because one cannot unlimitedly increase the size of the pump beam (or unlimitedly decrease the sizes of the signal and idler beams). Moreover, for small w_s and w_i , the pixelation effects of the SLMs cannot be neglected in the detection of the two-photon states. Under a typical experimental scenario with $\gamma \sim 1$ [22], entanglement concentration is inefficient to produce high-dimensional OAM-based MESs because of its narrow spiral bandwidth. In contrast, by shaping the radial components p of the pump light, we can considerably enhance the coincidence rate with $\gamma = 1$. Figure 4(a) compares the coincidence rates of above two methods under different value of γ for 10D, 15D, and 20D OAM-based MESs. The fidelities of our method are given in Fig. 4(b). Here, the coincidence rate of the entanglement concentration method is calculated with a pump light of $l_p = p_p = 0$. Clearly, for small γ and large d , the proposed pump shaping method is remarkably efficient.

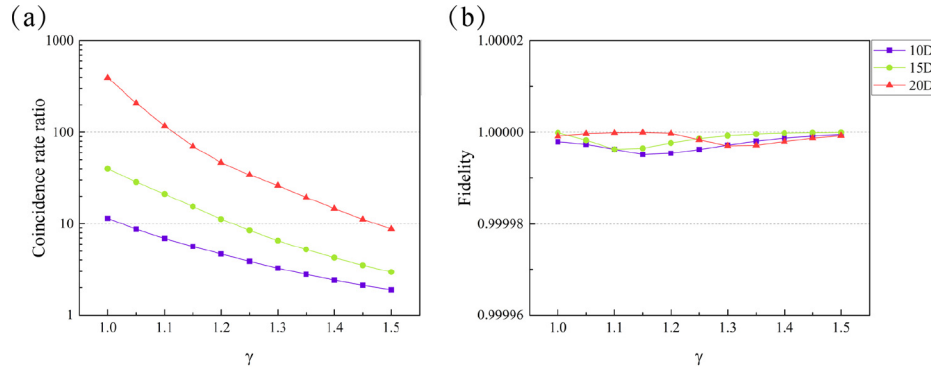


Fig. 4. (a) The dependence of the coincidence rate ratio of our method to entanglement concentration on γ . (b) The fidelities of 10D (purple), 15D (green), and 20D (red) OAM-based MESs in our method under different γ .

When the pump light consists of seventeen p components of LG pump light, we can produce in theory a 101D OAM-based MES with a fidelity of 0.999996 [Fig. 5(a)]. This result suggests that ultrahigh-dimensional OAM-based MESs can be produced by increasing the p components of the LG pump light. Interestingly, by utilizing the symmetry of the matrix A , we can produce specific entangled states featuring symmetric weight distributions. Figure 5(b) shows three states with their weight distributions having square, peaked, and funnel-shaped profiles, which demonstrate the versatility of our scheme for quantum state engineering.

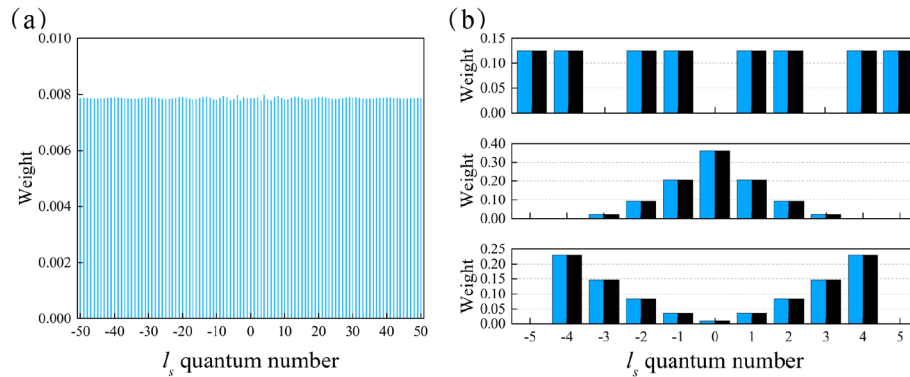


Fig. 5. (a) Normalized spiral spectrum of 101D OAM-based MES in the detection base. (b) Normalized entangled states with symmetric weight distributions. Black and blue bars denote the modes of the target and desired states, respectively.

Our method can also be applied to generate high-brightness high-dimensional MESs with OAM state being defined by $|\psi\rangle = \sum_{l_s, l_i} C_{l_s, l_i} |l_s\rangle |l_i\rangle$. Here, $C_{l_s, l_i} = \sum_{p_s, p_i} C_{p_s, p_i}^{l_s, l_i}$. In the numerical calculations, we use LG components of the pump light having mode indices of $p_p = 0, 1, \dots, 5$ and $l_p = 0$. The spatial modes of the coincidence detection base are $\gamma_s = \gamma_i = \gamma = 1$, $l_s, l_i = -50, -49, \dots, 50$ and $p_s, p_i = 0, 1, \dots, 10$. Figure 6(a) shows the normalized spectra of the coincidence probability amplitudes with $p_p = 0, 1, \dots, 5$. Figure 6(b) shows the corresponding d -dimensional OAM MESs. Here, $d = 3, 4, \dots, 20$. Figure 6(c) shows the calculated fidelity and coincidence rate. Clearly, the coincidence rate in this case can be significantly improved after optimizing the pump light through our method.

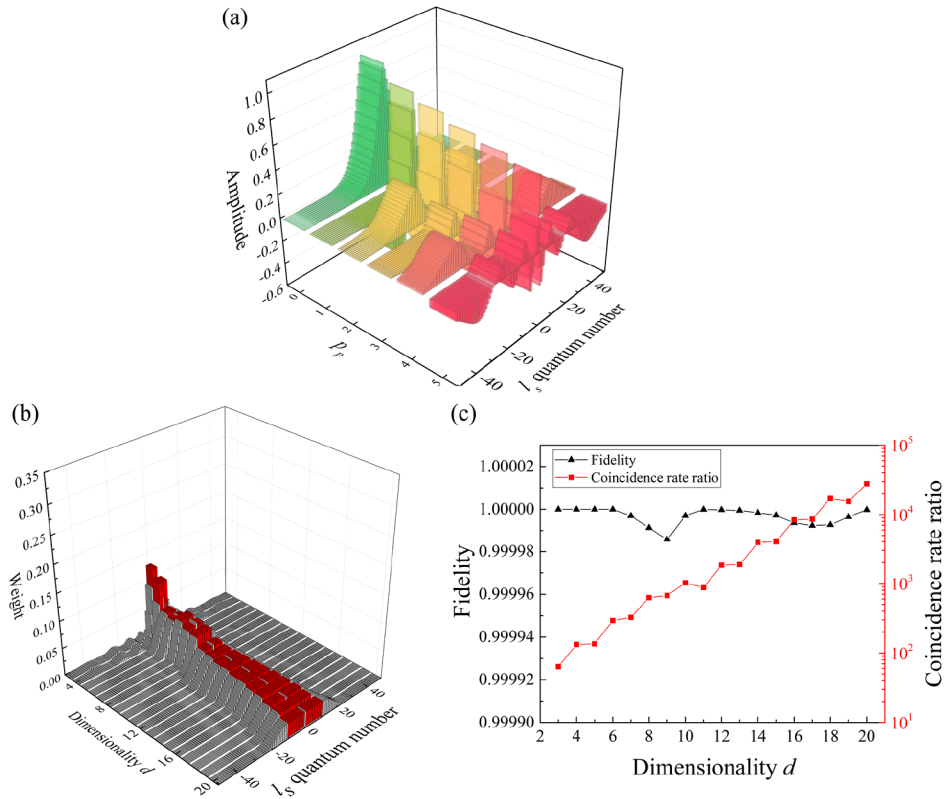


Fig. 6. (a) Normalized spectra of the coincidence probability amplitudes of $|\psi\rangle = \sum C_{l_s, l_i} |l_s\rangle |l_i\rangle$ with $l_p = 0$ and $p_p = 0, 1, \dots, 5$. (b) Normalized spiral spectra of the output states $|\psi\rangle_O$. Here, $d = 3, 4, \dots, 20$. Note that the normalization is performed on each detection base. Red bars denote the desired modes. (c) The fidelity between \tilde{O} and \tilde{T} and the ratio of the coincidence rate of our method to that of entanglement concentration. Here, $l_p = p_p = 0$ and $\gamma = 1$, and the detection base of entanglement concentration maintains $p_s = p_i = 0$.

4. Conclusion

To date, the highest quantum number of an OAM entangled state is 10010 [36], which indicates its great potential for increasing the capacity of quantum information processing. Using OAM correlation, researchers have realized quantum spiral imaging and pattern recognition [37–39], precision measurements [40,41], and combining and converting different physical degrees of freedom [42,43]. High-dimensional OAM-based MESs could further improve the performance of quantum states in these applications. With properly shaping the LG radial components of pump light, we propose a theoretical scheme to generate efficiently high-dimensional OAM-based MESs for quantum communication networks. Our method is also capable to realize quantum state engineering such as generation of OAM-entangled states with specific symmetric weights.

Funding. National Key Research and Development Program of China (2017YFA0303703, 2019YFA0308704); National Natural Science Foundation of China (11874212, 11874213, 11904424, 91950206); Fundamental Research Funds for the Central Universities (021314380105, 021314380191).

Disclosures. The authors declare no conflicts of interest.

Data availability. Data underlying the results presented in this paper are not publicly available at this time but may be obtained from the authors upon reasonable request.

References

1. M. Mafu, A. Dudley, S. Goyal, D. Giovannini, M. McLaren, M. J. Padgett, T. Konrad, F. Petruccione, N. Lütkenhaus, and A. Forbes, "Higher-dimensional orbital-angular-momentum-based quantum key distribution with mutually unbiased bases," *Phys. Rev. A* **88**(3), 032305 (2013).
2. D. Collins, N. Gisin, N. Linden, S. Massar, and S. Popescu, "Bell Inequalities for Arbitrarily High-Dimensional Systems," *Phys. Rev. Lett.* **88**(4), 040404 (2002).
3. S. Ecker, F. Bouchard, L. Bulla, F. Brandt, O. Kohout, F. Steinlechner, R. Fickler, M. Malik, Y. Guryanova, R. Ursin, and M. Huber, "Overcoming Noise in Entanglement Distribution," *Phys. Rev. X* **9**(4), 041042 (2019).
4. H. Jin, P. Xu, X. W. Luo, H. Y. Leng, Y. X. Gong, W. J. Yu, M. L. Zhong, G. Zhao, and S. N. Zhu, "Compact Engineering of Path-Entangled Sources from a Monolithic Quadratic Nonlinear Photonic Crystal," *Phys. Rev. Lett.* **111**(2), 023603 (2013).
5. L. Li, Z. Liu, X. Ren, S. Wang, V.-C. Su, M.-K. Chen, C. H. Chu, H. Y. Kuo, B. Liu, W. Zang, G. Guo, L. Zhang, Z. Wang, S. Zhu, and D. P. Tsai, "Metalens-array-based high-dimensional and multiphoton quantum source," *Science* **368**(6498), 1487–1490 (2020).
6. M. Kues, C. Reimer, P. Roztocky, L. R. Cortés, S. Sciara, B. Wetzels, Y. Zhang, A. Cino, S. T. Chu, B. E. Little, D. J. Moss, L. Caspani, J. Azaña, and R. Morandotti, "On-chip generation of high-dimensional entangled quantum states and their coherent control," *Nature* **546**(7660), 622–626 (2017).
7. A. C. Dada, J. Leach, G. S. Buller, M. J. Padgett, and E. Andersson, "Experimental high-dimensional two-photon entanglement and violations of generalized Bell inequalities," *Nat. Phys.* **7**(9), 677–680 (2011).
8. F. Brandt, M. Hiekkamäki, F. Bouchard, M. Huber, and R. Fickler, "High-dimensional quantum gates using full-field spatial modes of photons," *Optica* **7**(2), 98–107 (2020).
9. Y. Chen, W. Zhang, D. Zhang, X. Qiu, and L. Chen, "Coherent Generation of the Complete High-Dimensional Bell Basis by Adaptive Pump Modulation," *Phys. Rev. Appl.* **14**(5), 054069 (2020).
10. L. Allen, M. W. Beijersbergen, R. J. C. Spreeuw, and J. P. Woerdman, "Orbital angular momentum of light and the transformation of Laguerre-Gaussian laser modes," *Phys. Rev. A* **45**(11), 8185–8189 (1992).
11. S. Trajtenberg-Mills, A. Karnieli, N. Voloch-Bloch, E. Megidish, H. S. Eisenberg, and A. Arie, "Simulating Correlations of Structured Spontaneously Down-Converted Photon Pairs," *Laser Photonics Rev.* **14**(3), 1900321 (2020).
12. D. Wei, C. Wang, X. Xu, H. Wang, Y. Hu, P. Chen, J. Li, Y. Zhu, C. Xin, X. Hu, Y. Zhang, D. Wu, J. Chu, S. Zhu, and M. Xiao, "Efficient nonlinear beam shaping in three-dimensional lithium niobate nonlinear photonic crystals," *Nat. Commun.* **10**(1), 4193 (2019).
13. N. V. Bloch, K. Shemer, A. Shapira, R. Shiloh, I. Juwiler, and A. Arie, "Twisting Light by Nonlinear Photonic Crystals," *Phys. Rev. Lett.* **108**(23), 233902 (2012).
14. Y. Chen, R. Ni, Y. Wu, L. Du, X. Hu, D. Wei, Y. Zhang, and S. Zhu, "Phase-Matching Controlled Orbital Angular Momentum Conversion in Periodically Poled Crystals," *Phys. Rev. Lett.* **125**(14), 143901 (2020).
15. C. Xu, S. Huang, Q. Yu, D. Wei, P. Chen, S. Nie, Y. Zhang, and M. Xiao, "Manipulating the orbital-angular-momentum correlation of entangled two-photon states in three-dimensional nonlinear photonic crystals," *Phys. Rev. A* **104**(6), 063716 (2021).
16. A. Mair, A. Vaziri, G. Weihs, and A. Zeilinger, "Entanglement of the orbital angular momentum states of photons," *Nature* **412**(6844), 313–316 (2001).
17. A. Vaziri, J.-W. Pan, T. Jennewein, G. Weihs, and A. Zeilinger, "Concentration of Higher Dimensional Entanglement: Quirits of Photon Orbital Angular Momentum," *Phys. Rev. Lett.* **91**(22), 227902 (2003).
18. J. P. Torres, Y. Deyanova, L. Torner, and G. Molina-Terriza, "Preparation of engineered two-photon entangled states for multidimensional quantum information," *Phys. Rev. A* **67**(5), 052313 (2003).
19. S. Liu, Z. Zhou, S. Liu, Y. Li, Y. Li, C. Yang, Z. Xu, Z. Liu, G. Guo, and B. Shi, "Coherent manipulation of a three-dimensional maximally entangled state," *Phys. Rev. A* **98**(6), 062316 (2018).
20. E. V. Kovlakov, S. S. Straupe, and S. P. Kulik, "Quantum state engineering with twisted photons via adaptive shaping of the pump beam," *Phys. Rev. A* **98**(6), 060301 (2018).
21. V. D. Salakhutdinov, E. R. Eliel, and W. Löffler, "Full-Field Quantum Correlations of Spatially Entangled Photons," *Phys. Rev. Lett.* **108**(17), 173604 (2012).
22. F. M. Miatto, A. M. Yao, and S. M. Barnett, "Full characterization of the quantum spiral bandwidth of entangled biphotons," *Phys. Rev. A* **83**(3), 033816 (2011).
23. S. Kirkpatrick, C. D. Gelatt, and M. P. Vecchi, "Optimization by Simulated Annealing," *Science* **220**(4598), 671–680 (1983).
24. V. Arrizón, U. Ruiz, R. Carrada, and L. A. González, "Pixelated phase computer holograms for the accurate encoding of scalar complex fields," *J. Opt. Soc. Am. A* **24**(11), 3500–3507 (2007).
25. J. P. Torres, A. Alexandrescu, and L. Torner, "Quantum spiral bandwidth of entangled two-photon states," *Phys. Rev. A* **68**(5), 050301 (2003).
26. A. M. Yao, "Angular momentum decomposition of entangled photons with an arbitrary pump," *New J. Phys.* **13**(5), 053048 (2011).

27. D. Giovannini, J. Romero, J. Leach, A. Dudley, A. Forbes, and M. J. Padgett, "Characterization of High-Dimensional Entangled Systems via Mutually Unbiased Measurements," *Phys. Rev. Lett.* **110**(14), 143601 (2013).
28. S. Liu, S. Liu, C. Yang, Z. Xu, Y. Li, Y. Li, Z. Zhou, G. Guo, and B. Shi, "Classical simulation of high-dimensional entanglement by non-separable angular-radial modes," *Opt. Express* **27**(13), 18363–18375 (2019).
29. E. Bolduc, N. Bent, E. Santamato, E. Karimi, and R. W. Boyd, "Exact solution to simultaneous intensity and phase encryption with a single phase-only hologram," *Opt. Lett.* **38**(18), 3546–3549 (2013).
30. A. D'Errico, F. Hufnagel, F. Miatto, M. Rezaee, and E. Karimi, "Full-mode characterization of correlated photon pairs generated in spontaneous downconversion," *Opt. Lett.* **46**(10), 2388–2391 (2021).
31. S.-L. Liu, Q. Zhou, S.-K. Liu, Y. Li, Y.-H. Li, Z.-Y. Zhou, G.-C. Guo, and B.-S. Shi, "Classical analogy of a cat state using vortex light," *Commun. Phys.* **2**(1), 75 (2019).
32. F. Bouchard, N. H. Valencia, F. Brandt, R. Fickler, M. Huber, and M. Malik, "Measuring azimuthal and radial modes of photons," *Opt. Express* **26**(24), 31925–31941 (2018).
33. Y. Zhang, F. S. Roux, M. McLaren, and A. Forbes, "Radial modal dependence of the azimuthal spectrum after parametric down-conversion," *Phys. Rev. A* **89**(4), 043820 (2014).
34. F. S. Roux and Y. Zhang, "Projective measurements in quantum and classical optical systems," *Phys. Rev. A* **90**(3), 033835 (2014).
35. S. Liu, Y. Zhang, C. Yang, S. Liu, Z. Ge, Y. Li, Y. Li, Z. Zhou, G. Guo, and B. Shi, "Increasing two-photon entangled dimensions by shaping input-beam profiles," *Phys. Rev. A* **101**(5), 052324 (2020).
36. R. Fickler, G. Campbell, B. Buchler, P. K. Lam, and A. Zeilinger, "Quantum entanglement of angular momentum states with quantum numbers up to 10,010," *Proc. Natl. Acad. Sci. U. S. A.* **113**(48), 13642–13647 (2016).
37. N. Uribe-Patarroyo, A. Fraine, D. S. Simon, O. Minaeva, and A. V. Sergienko, "Object Identification Using Correlated Orbital Angular Momentum States," *Phys. Rev. Lett.* **110**(4), 043601 (2013).
38. L. Chen, J. Lei, and J. Romero, "Quantum digital spiral imaging," *Light: Sci. Appl.* **3**(3), e153 (2014).
39. X. Qiu, D. Zhang, W. Zhang, and L. Chen, "Structured-Pump-Enabled Quantum Pattern Recognition," *Phys. Rev. Lett.* **122**(12), 123901 (2019).
40. Y. Ming, J. Tang, Z. Chen, F. Xu, L. Zhang, and Y. Lu, "Generation of N00N State With Orbital Angular Momentum in a Twisted Nonlinear Photonic Crystal," *IEEE J. Select. Topics Quantum Electron.* **21**(3), 225–230 (2015).
41. W. Zhang, D. Zhang, X. Qiu, and L. Chen, "Quantum remote sensing of the angular rotation of structured objects," *Phys. Rev. A* **100**(4), 043832 (2019).
42. R. Fickler, R. Lapkiewicz, M. Huber, M. P. J. Lavery, M. J. Padgett, and A. Zeilinger, "Interface between path and orbital angular momentum entanglement for high-dimensional photonic quantum information," *Nat. Commun.* **5**(1), 4502 (2014).
43. J. T. Barreiro, N. K. Langford, N. A. Peters, and P. G. Kwiat, "Generation of hyperentangled photon pairs," *Phys. Rev. Lett.* **95**(26), 260501 (2005).